NANO LETTERS

2005
Vol. 5, No. 11
2144−2148

Creating Focused Plasmons by Noncollinear Phasematching on Functional Gratings

H. L. Offerhaus,* B. van den Bergen, M. Escalante, F. B. Segerink, J. P. Korterik, and N. F. van Hulst†

Applied Optics group, MESA+ Institute for Nanotechnology, University of Twente, The Netherlands

Received August 2, 2005; Revised Manuscript Received October 5, 2005

ABSTRACT

We report on the concept, generation, and first observations of focused surface plasmons on shaped gratings. The grating patterns are designed to realize focusing and directing through noncollinear phasematching. The plasmons are generated on patterned gold surfaces, and the plasmon propagation is observed using phase-sensitive photon scanning tunneling microscopy (PSTM) to extract the propagation pattern, direction, and wavelength.

Surface plasmon polaritons (plasmons for short) are enjoying an intense current interest in relation to left-handed materials,[1] enhanced transmission through subwavelength holes,[2] and even as (temporary) carriers of entanglement.[3] The combination of optical frequencies and the charge density nature of the wave allows for highly confined excitation and holds promise for nano-optical integrated circuits.[4] Despite the fact that they have been used as sensitive surface sensors for some time,[5] their appearance (or lack thereof) still creates strong debate about basic properties and issues.[6]

Plasmons play a particularly important role in light−matter interactions at the nanometer scale. The conversion of a light wave to a charge density wave allows the confinement far below the diffraction limit, paving the way for nanoscale plasmonic devices. A crucial factor for such circuitry is the efficient conversion of the large-scale incident light to the compressed or focused plasmonic wave. So far, the proven Kretschmann[7] configuration is used commonly to launch the plasmons on a large area that is then tapered to reduce the size.[8,9] Recently, an array of holes was used to demonstrate the possibility of focusing plasmons when they are created with the appropriate relative phase.[10] Similarly, plasmons created on an appropriately shaped ridge were shown to focus.[11] In those experiments, however, a very large area was illuminated to generate plasmons from only a very small portion of the surface.

In this paper, we present controlled generation of full 2D plasmon fields; by modulating the surface on which the plasmons are created, we engineer the direction in which they are generated for each position on the surface. We do not need to create the plasmons first and deflect them afterward but directly generate the plasmons in the desired pattern. Because plasmons have a very limited propagation length, the ability to generate the plasmons in the desired patterns has immediate advantages over separated steering and confinement. Figure 1 shows an example of such a surface modulation.

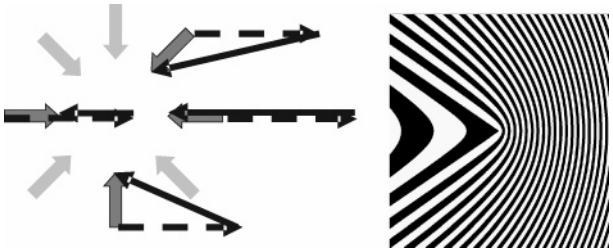

Figure 1. Creation of a full plane of focused plasmons through noncollinear phasematching. The left side shows the phasematching vectors, and the right side shows the resulting grating pattern. The dashed vectors correspond to the incident light (same everywhere), the gray vectors indicate the focused plasmons (converging toward center from everywhere), and the black continuous vectors indicate the required local grating vector.

We demonstrate the plasmon propagation on the metal surface by phase-sensitive PSTM, revealing the controlled noncollinear phase matching for all directions. The phase-sensitive technique allows us to extract the propagation pattern, direction, and wavelength on any point on the surface. This local imaging of the direction and amplitude is essential to provide the full view of plasmon propagation on the nanoscale.

* Corresponding author. E-mail: h.l.offerhaus@tn.utwente.nl.
† Present address: ICFO Institut de Ciències Fotoniques, Barcelona, Spain.

10.1021/nl0515089 CCC: $30.25
Published on Web 10/19/2005

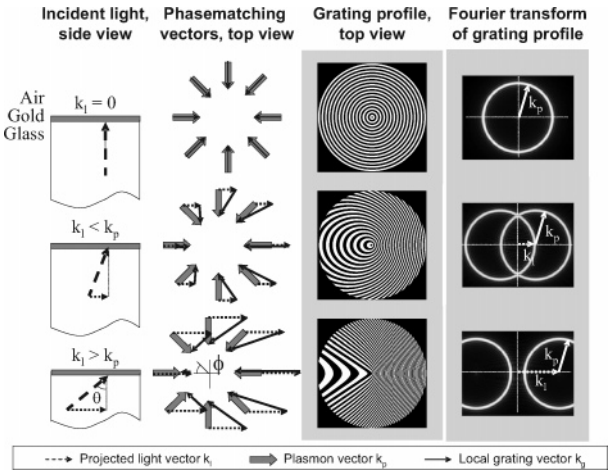

Figure 2. Concept of plasmon focusing through noncollinear phasematching. The grating profiles required for plasmon focusing and their Fourier transform are shown for different angles (θ) of incidence of the generating light. The top row shows normal incidence ($\theta = 0$), the middle row is for $k_l < k_p$, and the lower row is for $k_l > k_p$.

Concept. To achieve functional plasmon generation, we introduce a new approach to the design of gratings and the use of noncollinear phasematching. The grating is used as a holographic intermediate to achieve phasematching between a featureless excitation beam and a desired complex pattern providing customized k vectors at each position. This approach to grating design has applications beyond the generation of plasmons such as the design of patterns for periodically poled crystals for frequency conversion. In general, the gratings do not have to be continuous. For a grating consisting of an array of indentations or holes, the lattice of the array yields an inverse lattice in k space with many possible grating vectors to match to. The coupling strength of each vector is determined by the Fourier component of that vector in the grating pattern. This type of matching to an array vector was used in entanglement transfer.[3] The concept of engineered phasematching in a 2D grating was explored recently in the context of quasiphase-matched frequency conversion in 2D poled lithium niobate crystals.[13] The bull's-eye structure has been examined for unpolarized light in the context of plasmon-assisted transmission through subwavelength apertures.[14]

Figure 2 explains the concept of continuous functional plasmon generation through noncollinear phasematching. For a given frequency of incident light, the plasmons have a wavevector (k_p) determined by material parameters; for our case of plasmons on a gold−air interface excited with a HeNe laser, the plasmon wavelength ($\lambda_p = (2\pi/k_p)$ is approximately 593 nm. For efficient generation of plasmons, phasematching is required.[12] The (vector) addition of the projected wavevector of the incident light (k_l) and the grating vector (k_g) has to equal the plasmon vector. When light strikes perpendicular ($\theta = 0$, Figure 2 top row) then $k_l = 0$ so that k_g must equal k_p. For focusing from all directions (ϕ) the plasmon vector, and thus the grating vector, should be pointing toward the center from all directions. The corresponding grating consists of concentric circles or a bull's-eye structure (with a period of the aforementioned 593 nm). When the incident light strikes the surface at an angle (Figure 2 middle row), the incident wave front has a phase variation with respect to the surface that can be expressed as the projected light vector k_l. This k_l is a constant across the incident plane for illumination with a wide featureless beam (plane wave). To generate plasmons that converge to a single center, the grating vector must compensate locally for the project light vector causing the grating vector to be shortened before the focus (larger grating period) and lengthened after the focus (smaller grating period). When the angle is increased so much that k_l exceeds k_p (Figure 2 bottom row), the grating vector goes through zero and the grating patterns contain a discontinuity. In the plane of the grating along the line perpendicular to the incident light vector, the grating spacing is always the same and equal to the plasmon wavelength.

The grating properties are reflected in the Fourier transform of the patterns. The transform of the bull's-eye consists primarily of a single ring in k space. For the tilted incidence, the Fourier transform corresponds to a shifted circle, shifted by the length of the projected light vector that it has to compensate for. When the pattern is written as a binary grating (two-level grating with a square profile), the grating is real and symmetric so that two circles are seen in the Fourier transform, shifted in opposite directions. At those values for ϕ where $k_p \perp k_g$, the grating period along k_p goes through infinity, corresponding to an asymptotic behavior in real space.

P polarization of the incident light is a prerequisite for excitation because the plasmons are a longitudinal oscillation. This implies that linearly polarized incident light will excite plasmons in a two-lobe (bow-tie or butterfly) pattern. The orientation of that pattern depends on the orientation of the polarization with respect to the pattern. For light polarized in the plane of incidence, the pattern will be oriented along the plane of incidence. Possible photonic band gap dispersion effects[16] due to propagation on the grating itself have been reported, but these effects were ignored in this study because it requires a resonance that could only affect a small part of the generated plasmons.

Measurements. Our samples consist of microscope slides coated with a thin layer of gold on a chromium adhesion layer (2 nm chromium and ~50 nm of gold coated through evaporation). The grating structures are created on the top side of the gold by focused ion beam milling. From SEM images, the grating depth is estimated at 20−25 nm. Surface reflection measurements were done to establish the existence of the characteristic plasmon dip and to roughly estimate the layer thickness (which shows up in the reflection modulation depth). We measured on 1D gratings first that were rotated in the plane of the grating (changing ϕ, for constant θ) to observe noncollinear plasmon generation and establish the correct material properties that determine the k vector for plasmon resonance.

The photon scanning tunneling microscope (PSTM, also known as NSOM or SNOM) was reported in detail before.[15] In brief, it is a raster scanning method for probing the local electric field using a tip with a subwavelength aperture (typically less than 100 nm). The tip is kept at a constant

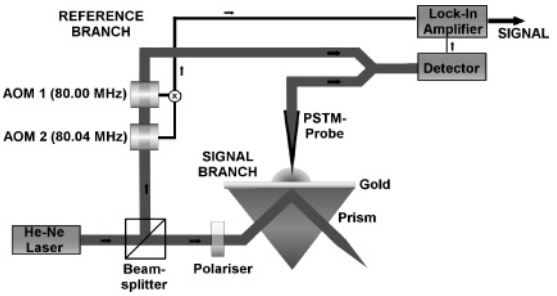

Figure 3. Experimental scheme for phase-sensitive PSTM. While scanning, the tip is kept at constant nanometric distance by shear force feedback. Mixing of the reference and signal branches allows for heterodyne interferometric detection of both amplitude and phase.

distance from the surface using a shear force feedback. For these measurements, the surface is raster scanned with a step size of typically 50 nm. For *phase-sensitive* PSTM, part of the excitation light is split off (see Figure 3) and sent through a reference arm where the frequency is shifted for heterodyne detection. The light in the reference arm is combined with light that is picked up from the sample. The beams are combined on a detector, and that signal is amplified in a lock-in amplifier to yield the amplitude and phase of the local light field. The combination of amplitude and phase allows the reconstruction of the field vector. This is, to the best of our knowledge, the first demonstration of phase-sensitive PSTM plasmon measurements on a metallic structure. We use a Kretchsmann-like setup[7] in which the light strikes the surface at an angle above the critical angle so that only evanescent waves are created and no direct transmission is observed. The microscope slide and prism are attached with a small amount of index matching fluid. The Kretschmann setup is not required for phasematching (provided by the gratings) but chosen because it reduces direct transmission, allows illumination and detection on separate sides, and provides relatively easy sample mounting.

To demonstrate different aspects of the noncollinear phase-matching, we present measurements on circular gratings using an inclined angle of incidence ($\theta \neq 0$). This is similar to measuring on 1D gratings rotated by ϕ for all values of ϕ simultaneously. These measurements show the phasematched generation of plasmons at specific values of (ϕ), corresponding to specific angles between the projected incoming light, the grating, and the generated plasmons. The measurements also show the change in the phase (by π) of the generated plasmons (with respect to the driving field). Finally, we present controlled focusing of plasmons on the stretched gratings. Observation of the phase shift and the propagation direction is not possible using only intensity PSTM; the phase information is crucial.

Results and Discussion. Figure 4 shows a typical measurement on a circular grating. The light from a HeNe laser strikes the surface through the glass at $\theta = 66°$ so that the projected k vector of the light (k_l) corresponds to a wavelength of 480 nm. The spot size of the HeNe is much larger than the grating area (several mm) so that the HeNe intensity on the surface is nearly constant. The periodicity of the circular grating is 700 nm and the plasmon wavelength

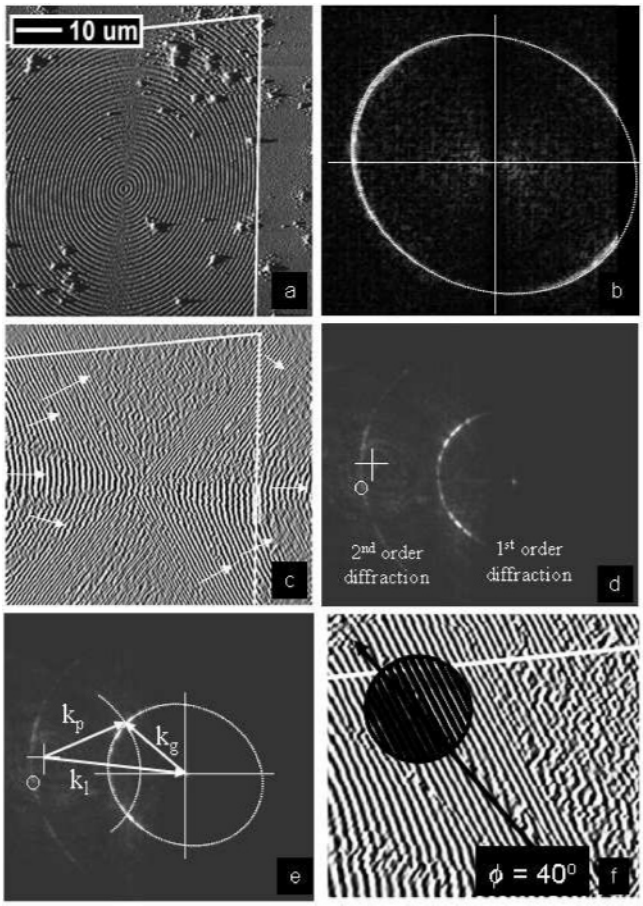

Figure 4. PSTM measurement on circular grating. The straight white lines in a, c, and f indicate the border of the grating. (a) Topography, (b) Fourier transform of the topography, (c) real part of the detected field, (d) Fourier transform of the (complex) field. (e) as d, (f) upper-left quadrant of the phase of the field.

is 593 nm. The three k vectors (k_l, k_g, and k_p) are thus of the same order of magnitude, with k_l roughly 1.8 times the size of k_g. Part a shows the topography of the surface as monitored through the shear force feedback. A slight nonorthogonality in scanning leads to the deformation from a square toward a parallelogram. Part b shows the Fourier transform of the grating with an overlay ellipse. Part c shows the real part of the (evanescent) optical field probed by the tip, expressed as amplitude times cos(*phase*). Examination of the progression of the phase through the measured pattern reveals the local direction of propagation indicated by the white arrows. Part d shows the Fourier transform of the probed (complex) field. The cross marked "0" indicates the zero spatial frequency. Part e is the same as d with added assignments. Indicated are the project light vector (k_l) running from 0 to the small dot. This light represents the unmodulated transmitted field. When the Fourier transform of the pattern in a is centered on the end of the light vector it perfectly overlaps with the measured circle section in the optical signal so that the circle section represents the modulated transmitted light. A second circle centered at 0 is added with a radius corresponding to the plasmon vector (k_p). At the crossing point of both circles, spots of increased intensity can be observed. Part f shows only the phase of the probed field in

the upper-left corner of the pattern. The slanted black line indicates $\phi = 40°$, the angle for which the plasmon resonance is expected. In the circle, a regular spaced raster pattern of black lines is overlaid to bring out the relative phase below and above the resonance line.

The grating structure on the surface of the gold introduces the modulation on the projected light to create the light field to drive the plasmon creation. This (evanescent) driving field is detected by the PSTM *independent* of the presence of plasmons. This driving field corresponds to the diffracted portion of the incoming light, the phase of which corresponds to the phase of the incoming light multiplied by the phase delay induced by the grating. The Fourier transform of that field thus corresponds to the convolution of the Fourier transform of the incoming light (a delta function) with the Fourier transform of the grating (largely a ring). The measured circle section in 4d indeed coincides exactly with the Fourier transform of the grating centered on the end of the projected light vector. We do not see the full ring because of limited resolution of the scanning. The phase of the driving field is determined only by the grating and the phase of the incident light so that it is continuous in the absence of resonances. Where the phasematching condition is fulfilled and the polarization contains a component along the propagation direction of the plasmons, resonant plasmons can be generated. An indication for resonant excitation is an increase in the amplitude of the detected field and a change in the phase of the oscillating charge. For this configuration, the plasmon resonance is expected at an angle of $\phi = 40°$ (and $\phi = -40°$) degrees. In 4c, wedge-shaped sections of higher amplitude can be seen around certain values for ϕ. Note that the part of the Fourier transform around $\phi = 40°$ contains contributions from the wedge sections of the upper left where waves are generated that travel toward the upper right-hand side and contributions from the wedge on the lower right-hand side, where waves are generated that also travel toward the upper right-hand side. The former wedge shape uses a k vector that points outward with respect to the local grating pattern, whereas the latter uses a k vector that points inward.

The waves of several of these sections of increased amplitude can be seen to extend beyond the grating boundary indicated by the solid white line, beyond the reach of the driving field, therefore indicating that these represent propagating waves. These high-intensity sections correspond to the bright dots on the circle section of the Fourier transform. The waves attenuate as they propagate away from the grating boundary, indicating a propagation length on the order of 10 μm. Figure 4f shows the π phase shift between the part below the resonance at $\phi = 40°$ degrees and the part above resonance. The overlaid raster is provided to guide the eye. The line where the phase shift is seen in space is the result of the interference of waves generated with different phases. The line is thus not observed at the position of the phase shift in the generation but shifted along the propagation direction of the waves to the point where sufficient field is generated at the new phase to compensate the field generated previously. The line at 40° thus does not pass through the center of the circle pattern but is shifted towards the upper

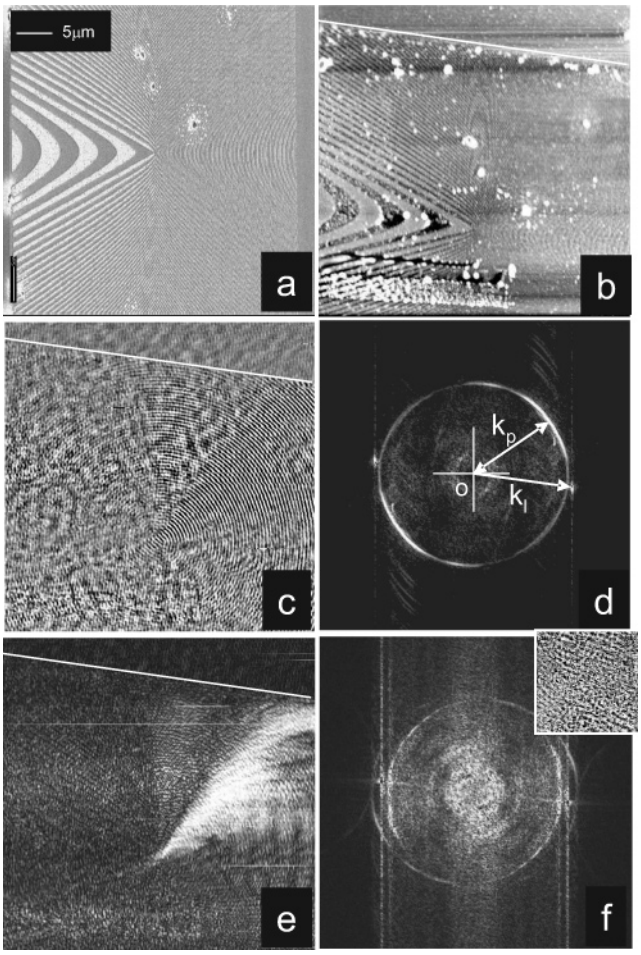

Figure 5. PSTM measurement on slanted grating design. (a) SEM image of grating, (b) topography of scan area, (c) real part of the field, (d) Fourier transform of c with vector assignments (note that k_l just exceeds the circle radius, k_p), (e) amplitude only, and (f) Fourier transform of measurement on same grating tilted away from resonance.

right-hand side. The line can be seen to extend all the way through the wedge section on the lower right-hand side. The (vertical) mirror of this line can also be seen, although that one is less clear because of the dust particles in those sections of the grating.

At smaller angles, other oscillations can be seen with a longer period. These longer wavelength oscillations are yet to be identified. They are not a grating artifact because they can be observed to extend beyond the grating. The wavelength does not correspond to a diffracting angle that could be picked up by the probe or to plasmons on the glass−gold interface. The wavelength also rules out reflected normal plasmons or light scattered by the surface corrugation. These waves were also observed in measurements on rotated (ϕ) 1D gratings but not in the surface reflection measurements where the low angle of reflection was outside our measuring range.

Figure 5 shows measurements on a gratings that is shifted in the Fourier domain to produce focused plasmons in real space. Part a shows a SEM image of the grating. Part b shows the topography of the measured area. Parts c−e show a measurement on the plasmon resonance. Here the polariza-

tion was rotated by 30°. The rotation of the pattern of the measured amplitude supports the fact that these are plasmons and not just diffractive modulation (polarization insensitive). However, damage to the grating prevented a systematic analysis of the pattern as a function of polarization direction. Part c depicts the real part of the measured signal. It clearly shows the circular wave fronts around a common center. Examination of the relative phase of the real and imaginary part of the signal shows that the plasmons are traveling toward the center, which can also be deduced from the fact that no waves are seen outside the grating boundary. Part d is the Fourier transform of c. This is the Fourier transform of the real part of the signal (not the complex Fourier transform) to emphasize the fact that the shape of the Fourier transform is a single ring (different from f where two rings can be seen). The projected light vector, k_l, can again be identified as a dot. The Fourier transform of the grating consists of circles shifted by slightly more than k_l. The convolution of the projected light and the grating thus produces one ring around the origin and a ring centered at almost two k_l. The second ring cannot be seen here, partly because it is not at resonance so that it does not produce much field, partly because the modulation exceeds the resolution of the scanning. Part e shows the amplitude only to highlight the region where plasmons are generated. Alignment was not yet perfect and repeated scanning caused localized damage to the grating, especially the lower right corner. The light comes in from the left so that the streak of plasmons visible in e is traveling against the incoming light. Most of the plasmon creation is on the part of the grating with a highly modulated pattern, experiencing many modulation periods over a short distance. Although the small plasmon propagation length on these samples limits the center intensity, the pattern clearly shows the generation of plasmons aimed at the common center. Part f shows the Fourier transform of the real part of the signal when the grating is tilted away from the plasmon resonance (different θ), yielding two shifted circles and highlighting the mismatch. The full (complex) Fourier transform shows only one circle, slightly shifted away from the center. By taking the Fourier transform of the real part of the signal, all signals are reflected around the origin and the shift of the circle from the center is readily visible, also for deformed circles. For further visibility of the rings, the dots corresponding to the directly transmitted light have been suppressed. These dots are much stronger compared to the signal in the measurements away from the resonance. The inset shows the real part of the field. Some streaks are still visible, but they are much weaker compared to the directly transmitted signal. This is what one would expect for a driving field that is a shifted circle next to a resonance that is a centered circle.

Conclusions. In conclusion, we have shown the first phase-sensitive PSTM measurements of the creation of directed plasmons on specifically engineered gratings. We expect that this direct focused creation of plasmons will be more efficient than creation followed by a directing step. We have demonstrated the strength of phase-sensitive PSTM to visualize the plasmon propagation on these surfaces. For future experiments, we will improve the gold surface to increase propagation lengths and intensity in the center. These patterns are based on a theory of propagation that considers only far-field components and therefore cannot be expected to focus the plasmons beyond the diffraction limit. It seems quite feasible, however, to add subwavelength (dispersive) features[17] to the center for further localization of the plasmon field to a few tens of nanometers. We believe that this method of directed plasmon creation opens up possibilities for efficient localized excitation sources at optical frequencies.

Acknowledgment. We acknowledge L. (Kobus) Kuipers for useful discussions, R. Engelen for his assistance on the scanning setup, and R. Kooyman for the use of reflection simulation software. This research is supported by NanoNed, a nanotechnology program of the Dutch Ministry of Economic Affairs.

References

(1) Pendry, J. *Nature* **2003**, *423*, 22−23.
(2) (a) Barnes, W. L.; Dereux, A.; Ebbesen, W. *Nature* **2003**, *424*, 824−830. (b) Ebbesen, T. W.; Lezec, H. J.; Ghaemi, H. F.; Thio, T.; Wolff, P. A. *Nature* **1998**, *391*, 667−669.
(3) Altewischer, E.; van Exter, M. P.; Woerdman, J. P. *Nature* **2002**, *418*, 304−306.
(4) Ditlbacher, H.; Krenn, J. R.; Schider, G.; Leitner, A.; Aussenegg, F. R. *Appl. Phys. Lett.* **2002**, *81*, 1762−1764.
(5) (a) Rothenhausler, B.; Knoll, W. *Nature* **1988**, *332*, 615−617. (b) Baksh, M. M.; Jaros, M.; Groves, J. T. *Nature* **2004**, *427*, 139−141.
(6) Lezec, H. J.; Thio, T. *Opt. Express.* **2004**, *12*, 3629−3651.
(7) Kretschmann, E. *Z. Phys.* **1971**, *241*, 313−324.
(8) Krenn, J. R.; Weeber, J. C. *Philos. Trans. Royal Soc. London, Ser. A* **2004**, *362*, 739−756.
(9) Hecht, B.; Bielefeldt, H.; Novotny, L.; Inouye, Y.; Pohl, D. W. *Phys. Rev. Lett.* **1996**, *77*, 1889−1892.
(10) Yin, L.; Vlasko-Vlasov, V. K.; Pearson, J.; Hiller, J. M.; Hua, J.; Welp, U.; Brown, D. E.; Kimball, C. W. *Nano Lett.* **2005**, *5*, 1399−1402.
(11) Liu, Z.; Steele, J. M.; Srituravanich, W.; Pikus, Y.; Sun, C.; Zhang, X. *Nano Lett.* **2005**, *5*, 1726−1729.
(12) Raether, H. *Surface Plasmons*; Springer-Verlag: Berlin, 1988.
(13) (a) Berger, V. *Phys. Rev. Lett.* **1998**, *81*, 4136−4139. (b) Broderick, N. G. R.; Ross, G. W.; Offerhaus, H. L.; Richardson, D. J.; Hanna, D. C. *Phys. Rev. Lett.* **2000**, *84*, 4345−4348.
(14) Lezec, H. J.; Degiron, A.; Devaux, E.; Linke, R. A.; Martin-Moreno, L.; Garcia-Vidal, F. J.; Ebbesen, T. W. *Science* **2002**, *297*, 820−822.
(15) (a) Balistreri, M. L. M.; Korterik, J. P.; Kuipers, L.; van Hulst, N. F. *JLT* **2001**, *19*, 1169−1176. (b) De Hollander, R. B. G.; van Hulst, N. F.; Kooyman, R. P. H. *Ultramicroscopy* **1995**, *57*, 263−269.
(16) Depine, R. A.; Ledesma, S. *Opt. Lett.* **2004**, *29*, 2216−2218.
(17) Stockman, M. I. Adiabatic Energy Concentration in Graded Nanoplasmonic Waveguides. In Conference on Lasers and Electro- Optics/ Quantum Electronics and Laser Science and Photonic Applications, Systems and Technologies, 2005; Optical Society of America: Washington, DC, 2005; QMK2.

NL0515089